NATIONAL ADVISORY COMMITTEE FOR AERONAUTICS

WARTIME REPORT

ORIGINALLY ISSUED
June 1942 as
Advance Restricted Report

THE CHARACTERISTICS OF TWO MODEL SIX-BLADE

COUNTERROTATING PUSHER PROPELLERS OF CONVENTIONAL

AND IMPROVED AERODYNAMIC DESIGN

By James G. McHugh and Edward Pepper

Langley Memorial Aeronautical Laboratory
Langley Field, Va.

NACA

WASHINGTON

NATIONAL ADVISORY COMMITTEE FOR AERONAUTICS

ADVANCE RESTRICTED REPORT

THE CHARACTERISTICS OF TWO MODEL SIX-BLADE
COUNTERROTATING PUSHER PROPELLERS OF CONVENTIONAL
AND IMPROVED AERODYNAMIC DESIGN

By James G. McHugh and Edward Pepper

SUMMARY

The aerodynamic characteristics of models of two counterrotating six-blade propellers are compared from the results of tests made in the NACA 19-foot pressure tunnel. One of the propellers, which is representative of a type now in use on military and commercial airplanes, embodies modified Clark Y airfoil sections in blades of thickness ratio and plan form dictated largely from considerations of structural reliability. The other propeller embodies NACA 16-series sections in blades of thickness ratio and plan form dictated largely from considerations of minimum aerodynamic losses.

The propellers differ in plan form, thickness ratio, diameter, section shape, and pitch distribution. Owing to the numerous variables involved, it is not possible to isolate the influence of each variable on the aerodynamic characteristics of the propellers tested. The results of this investigation show, however, that higher values of propulsive efficiency may be obtained from propellers designed from consideration of minimum aerodynamic losses than can be obtained from propellers of conventional design. At the relatively low airspeeds at which the tests were conducted, the gain in propulsive efficiency varied from 1.5 to 4.0 percent, depending on the pitch of the propeller. It is believed likely that greater differences may be obtained at high airspeeds.

INTRODUCTION

The selection of propellers that meet the operating requirements of modern airplanes involves numerous problems. The propeller must develop suitable take-off char-

acteristics at sea level and must also efficiently absorb
the power output of the engine at high forward speeds in
rarefied air at high altitudes. Such operating require-
ments make it difficult to avoid large rotational and
compressibility losses of the propellers.

Previous investigations show that the rotational
losses of high-pitch propellers may be materially reduced,
if not wholly eliminated, by the use of counterrotating
propellers. The advantages of such propeller arrangements
are discussed in references 1 and 2.

At high forward speeds a large portion of the pro-
peller blade operates at high values of Mach number. If
the blade sections operate at resultant velocities at
or above their critical speed, the drag losses may be
extremely high. The resultant velocities at which the
blade sections operate may, to some extent, be controlled
to allow for operation below critical speeds through suit-
able compromises in the selection of the rotational speed,
the diameter, and the solidity of the propeller. A further
step in the solution of the problem is to increase the
critical speed of the propeller by incorporating blade
sections designed to delay the compressibility burble.
(See reference 3.)

It is of general interest, therefore, that comparative
data be obtained regarding the characteristics of various
arrangements of counterrotating propellers. This paper
presents the results of a comparison of two arrangements
of models of six-blade counterrotating pusher propellers,
one of a conventional design that embodies modified Clark
Y airfoil sections (reference 4) and the other of a design
that produces minimum induced losses and embodies NACA
16-series airfoil sections that delay the compressibility
burble.

The two arrangements of models of six-blade counter-
rotating pusher propellers were investigated at blade
angles of approximately 20°, 30°, 40°, 45°, 50°, 55°,
and 60° at 0.75 of the tip radius. The tests were con-
ducted at airspeeds that ranged from 60 to 150 miles per
hour. The results are not, therefore, indicative of the
compressibility effects that may be expected from full-
scale propellers operating at high forward speeds.

APPARATUS AND METHODS

The investigation was conducted at atmospheric
pressure in the NACA 19-foot pressure tunnel. Scale models

of two arrangements of counterrotating propellers were tested. The propellers differed in section shape, plan form, thickness ratio, and pitch distribution.

One propeller of conventional design, hereinafter referred to as propeller 512, is similar to the full-scale Curtiss propeller 512 and embodies modified Clark Y airfoil sections. Both the forward and the rear propeller of the counterrotating pair were 45 inches in diameter.

The other propeller, hereinafter referred to as propeller 4-308-045, embodies NACA 16-series airfoil sections. Its aerodynamic design is based on Goldstein's modification of the vortex theory of propellers (reference 5) and the plan form was made to conform to the condition of optimum blade loading, that is, minimum induced losses, for a single-rotating propeller of pitch-diameter ratio of 2.17.

Neither propeller was specifically designed for counterrotating operation. Figure 1 shows, for both propellers, the blade-form curves and the geometric-pitch distribution for several blade-angle settings. A photograph showing the plan forms is given as figure 2.

The propellers were tested on a scale model of an airplane equipped for counterrotating pusher propellers. Figures 3 and 4 show the propellers assembled on the model. The general dimensions of the propeller test arrangement are shown in figure 5. The attitude of the model was adjusted to make the thrust line horizontal and, in this position, the lift coefficient was approximately equal to zero.

Each propeller of the counterrotating pair was driven by an individual water-cooled, alternating-current induction motor rated 50 horsepower at 3500 rpm. The two motors were in tandem with one motor driving through the hollow shaft of the other motor. Current was supplied to the motors by a variable-frequency alternator and the speed was controlled by variation of the frequency. With this arrangement the power delivered to each propeller was determined from a calibration involving motor torque, speed of revolution, and active current.

The blade angles of the propeller were set on a propeller table with templets accurately fitted for each blade. The protractor accuracy is within ±0.1°.

Conventional propeller test procedure was used through a range of V/nD values for each blade setting. Constant maximum torque was maintained and the tunnel and the propeller speeds were increased in any desired increment until the tunnel speed reached a maximum of 150 miles per hour. At this tunnel speed, the propeller speed was then reduced to reach higher values of V/nD. Approximate values of propeller and tunnel speeds had been predetermined for a suitable distribution of V/nD values for the test points. The values of thrust and power measured were converted to nondimensional coefficients and plotted as a function of V/nD.

Typical test results are presented in figure 6 and it is believed that the accuracy of the faired curves as indicated by the scatter of the test points is within three-fourths of 1 percent throughout the greater part of the test range.

An effort was made to maintain equal power absorption and equal rotational speed for the two counterrotating propellers. This procedure was impractical, however, for all operating conditions and, as a practical expedient, the condition of equal power absorption and equal rotational speed was restricted to the propeller operating range in the region of peak propulsive efficiency. The pitch of the front propeller was set at a predetermined value and the pitch of the rear propeller was adjusted to make its rotational speed and power absorption equal to those of the front propeller at the operating conditions in the region of peak efficiency. The difference in blade angles of the front and rear propellers required for this condition is shown in figure 7. In certain instances the region of equal power absorption varied somewhat from the region of peak efficiency. These differences are believed not to be sufficiently important to change appreciably the measured values of maximum efficiency.

SYMBOLS AND COEFFICIENTS

The symbols and coefficients used in the report are defined as follows:

C_T thrust coefficient $\left(\dfrac{T - \Delta D}{\rho n^2 D^4} \right)$

T total thrust of propellers (compression in propeller shafts)

ΔD change in body drag due to action of propellers

ρ mass density of air

n rotational speed of rear propeller

D $\dfrac{(\text{diam. front prop.}) + (\text{diam. rear prop.})}{2}$

C_{P_T} total-power coefficient $\left(C_{P_F} + C_{P_R} \right)$

C_{P_F} power coefficient of front propeller $\left(\dfrac{P_F}{\rho n^3 D^5} \right)$

C_{P_R} power coefficient of rear propeller $\left(\dfrac{P_R}{\rho n^3 D^5} \right)$

P_F power supplied to front propeller

P_R power supplied to rear propeller

$P_T = P_F + P_R$

η propulsive efficiency $\left(\dfrac{(T - \Delta D)V}{P_T} \right)$

V velocity of the air stream

V/nD advance-diameter ratio

C_s speed-power coefficient $\left(\sqrt[5]{\dfrac{\rho V^5}{P_T n^2}} \right)$

M Mach number $\left(\dfrac{\text{resultant tip speed}}{\text{velocity of sound}} \right)$

β propeller blade angle at 0.75 radius

RESULTS AND DISCUSSION

The efficiency curves for propeller 4-308-045 are presented in figure 8 for the several blade-angle settings

investigated. Figures 9 and 10 show the thrust and the total-power coefficients. The individual power coefficients are given in figure 11. A design chart showing the variation of propulsive efficiency and V/nD with the speed-power coefficient is presented in figure 12.

The efficiency, thrust, and total-power coefficients of propeller 512 are presented in figures 13, 14, and 15, respectively. The individual power curves and the design chart for this propeller are shown in figures 16 and 17, respectively.

Limitations of the minimum speed and of the power output of the motors that drove the propellers made it impossible to investigate thoroughly the characteristics of the propellers operating in a low V/nD range. All comparisons of these results must be limited, therefore, to the range of operating conditions in the vicinity of peak efficiency. The general trends that are believed, however, to exist in the low range of V/nD are represented by dashed lines in the faired curves of thrust, power, and efficiency.

The efficiency envelopes of propeller 4-308-045 and propeller 512 are compared in figure 18. The efficiency of propeller 4-308-045 is higher than the efficiency of propeller 512 by an amount that varies from one-half of 1 percent at a V/nD of 1.5 to 4 percent at a V/nD of 3.4. The differences in propulsive efficiency increase proportionately with blade-angle setting until the region of maximum efficiency is reached. Beyond that region the difference in efficiencies throughout the rest of the V/nD range is approximately constant. With regard to the values of efficiency obtained with propeller 512, attention is called to the results of reference 6, which show, from low-speed tests of full-scale single-rotating tractor propellers of approximately the same general blade form as propeller 512, that the addition of suitable shank fairings to such propellers yields a gain in propulsive efficiency of approximately 2 percent at $\beta = 45°$ and approximately 6 percent at $\beta = 60°$. On the basis of the results of reference 6 it would appear that the addition of suitable shank fairings to propeller 512 might have resulted, therefore, in an increase in its propulsive efficiency.

The effect of the blade-shank shape and the low drag sections of propeller 4-308-045 may be seen by a comparison of the efficiency curves of the two propellers (fig. 19). The extended crest in the efficiency curves for propeller

L-404

4-308-045 shows lower drag shank and blade sections. A greater difference in the efficiency envelopes and curve forms would probably occur at higher resultant velocities. Owing to the high critical speed of the NACA 16-series sections, the advantages of propellers embodying these sections would probably be more pronounced at values of Mach numbers greater than 0.75. In this series of tests the maximum value of M attained with propeller 4-308-045 was 0.58 and the maximum M attained with propeller 512 was 0.628. Greater differences in the efficiencies of the two propellers would be expected at full-scale high-speed operation.

In a comparison of the characteristics of propeller 4-308-045 and propeller 512, thrust and power absorption are important. These factors depend to a great extent upon plan form, pitch distribution, thickness ratio, diameter, and propeller-blade sections. Any interpretation of results must, therefore, take into consideration the fact that the propellers compared differed in these respects.

The total power absorption of propeller 4-308-045 was greater than that of propeller 512. The difference ranged from approximately 15 percent at low blade angles to approximately 25 percent at high blade angles. The ratios of the power absorption of the two propellers at their peak efficiency operating condition are shown in figure 18. The greater power absorption of propeller 4-308-045 may be largely attributed to the fact that its blade area is approximately 25 percent greater than that of propeller 512.

CONCLUSIONS

At the low values of airspeed at which this investigation was conducted, the maximum values of propulsive efficiency obtained with propeller 4-308-045 were greater than those obtained with propeller 512 by an amount that varied from one-half of 1 percent at a V/nD of 1.5 to 4 percent at a V/nD of 3.4. The greater efficiency of propeller 4-308-045 is attributed to the fact that it is designed to produce minimum aerodynamic losses, whereas the design of propeller 512 was dictated largely from considerations of structural reliability.

Propeller 4-308-045, because of greater blade area, absorbs more power than propeller 512.

Langley Memorial Aeronautical Laboratory,
    National Advisory Committee for Aeronautics
        Langley Field, Va.

8

REFERENCES

1. Biermann, David, and Hartman, Edwin P.: Wind-Tunnel Tests of
   Four- and Six- Blade Single- and Dual-Rotating Tractor
   Propellers. NACA Rep. No. 747, 1942.

2. Stickle, George W., and Crigler, John L.: Propeller Analysis
   from Experimental Data. NACA Rep. No. 712, 1941.

3. Stack, John: Tests of Airfoils Designed to Delay the
   Compressibility Burble. NACA TN No. 976, Dec. 1944.
   (Reprint of ACR, June 1939.)

4. Biermann, David, and Hartman, Edwin P.: The Effect of
   Compressibility on Eight Full-Scale Propellers Operating in
   the Take-Off and Climbing Range. NACA Rep. No. 639, 1938.

5. Lock, C. N. H.: The Application of Goldstein's Theory to the
   Practical Design of Airscrews. R. & M. No. 1377,
   British A.R.C., 1932.

6. Biermann, David, and Pepper, Edward: Tests of Several
   Propeller Cuffs Designed for Different Loadings. NACA A.R.R.,
   Feb. 1942.

L-404
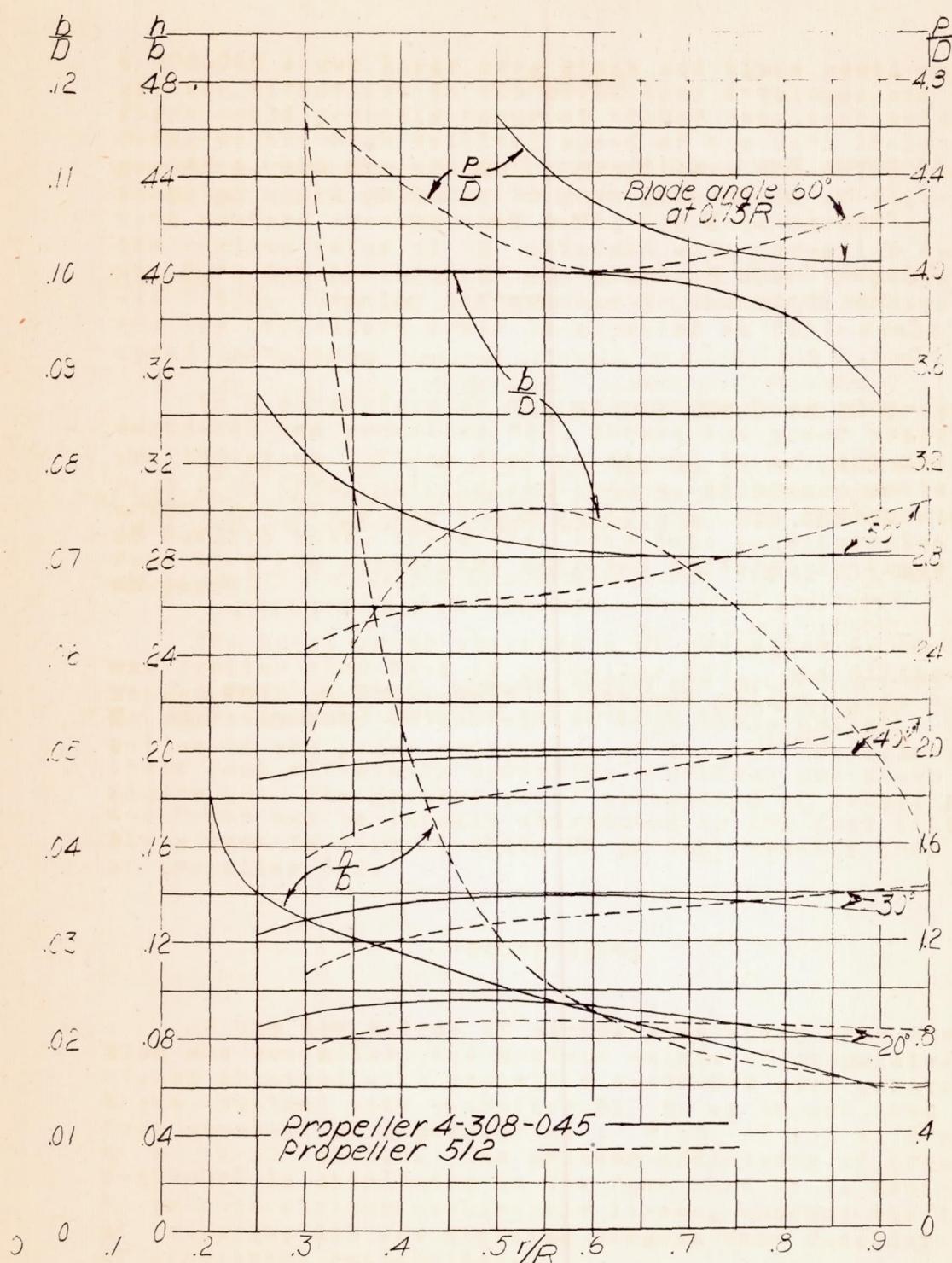
Figure 1.— Blade-form curves for propellers
4-308-045 and 512.   D, diameter; R, radius to tip;
r, station radius; b, section chord; h, section thickness;
p, geometric pitch of section chord line.

(a) Propeller 512.   (b) Propeller 4-308-045.
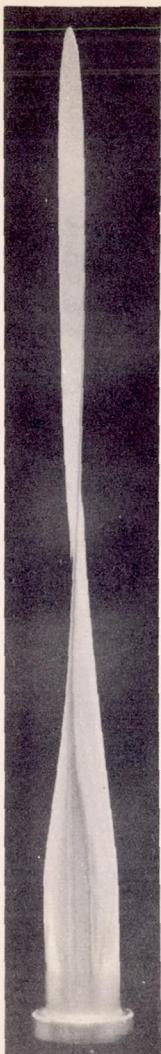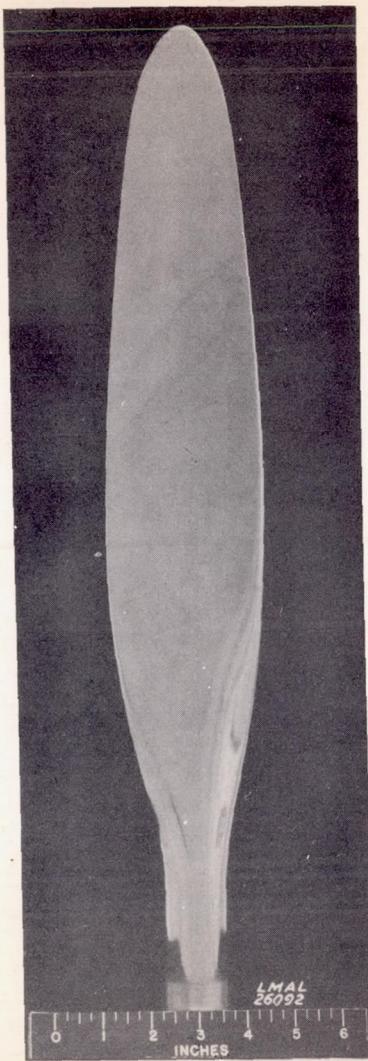
Figure 2.- Plan-form and trailing-edge views.

Fig. 2
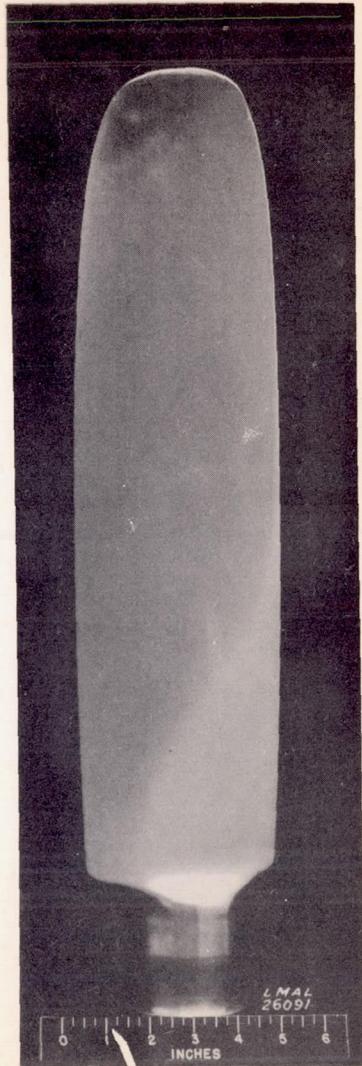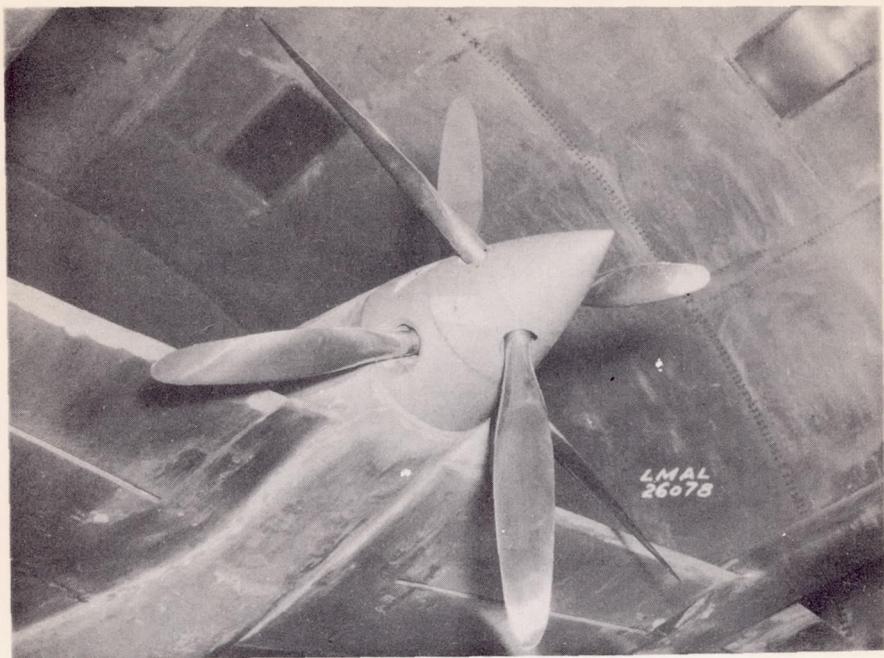
Figure 3.- Assembly of propeller 512 on model.
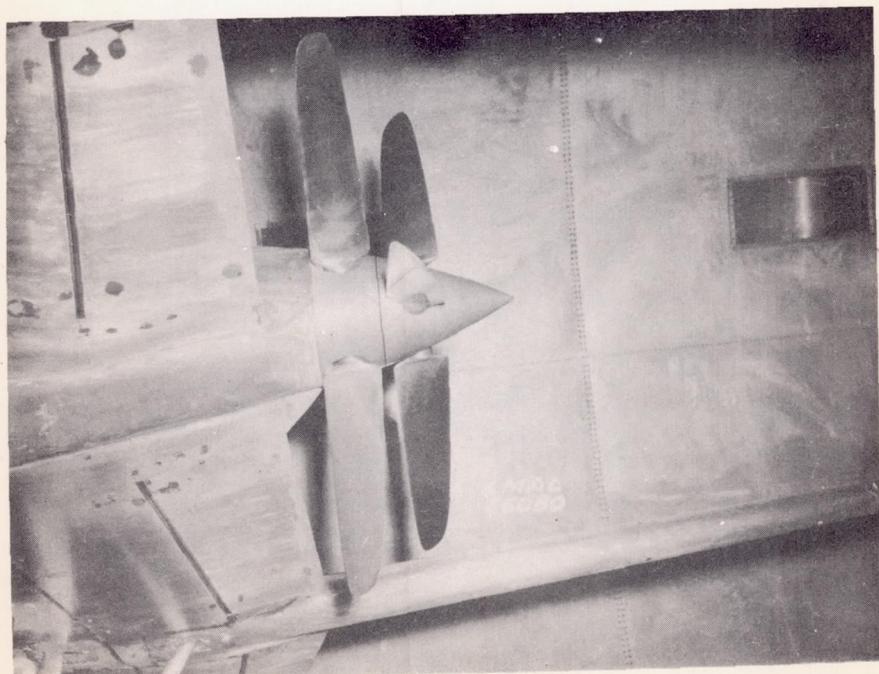
Figure 4.- Assembly of propeller 4-308-045 on model.

	D_F	D_R
Curtiss 512	45"	45"
NACA 4-308-045	47.462"	46.456"

16.000"

5.625"

D_F

10.375"

7.43"

D_R

Thrust line

Wing

5.682"

₵ ₵
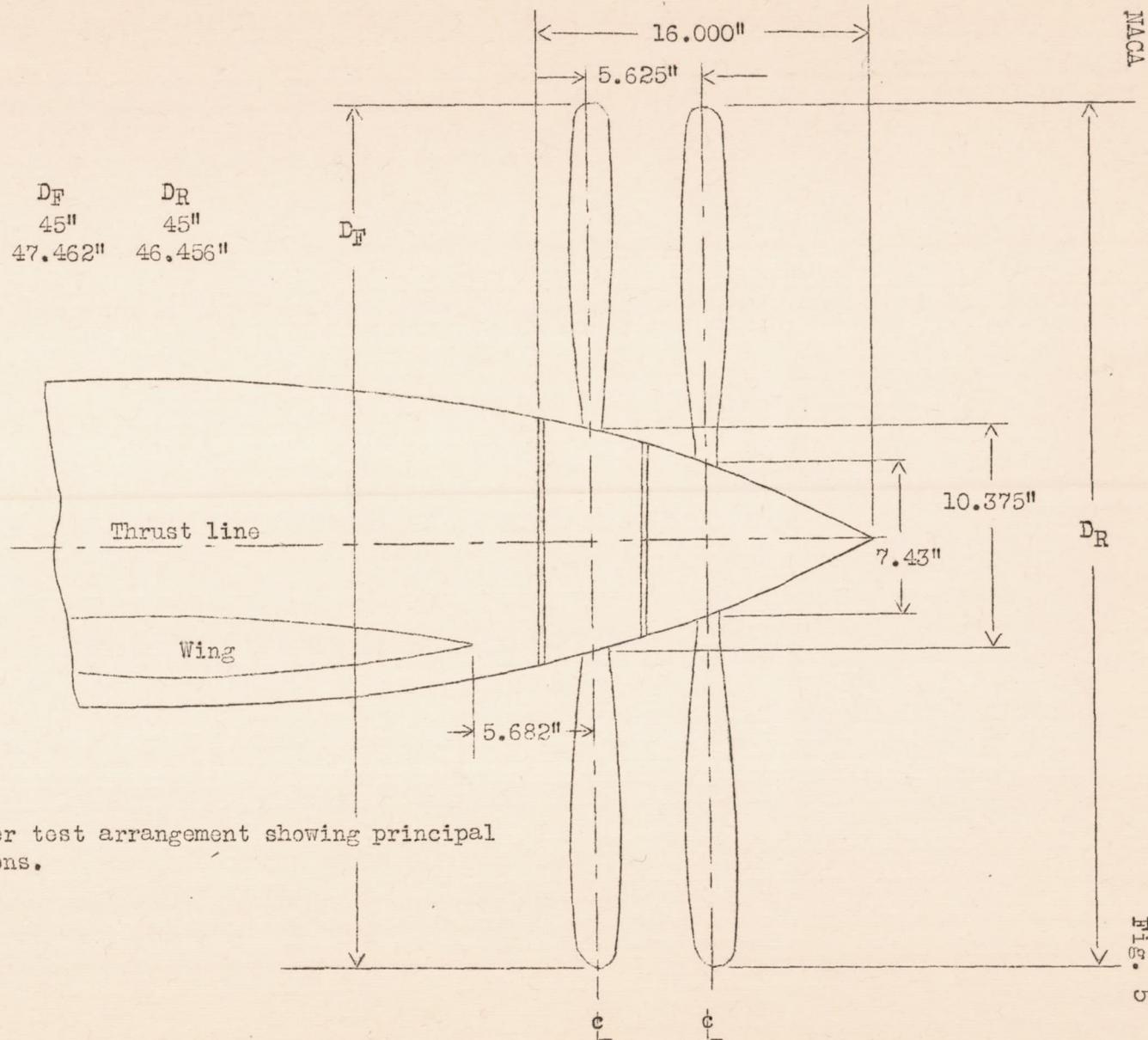
Figure 5.- Propeller test arrangement showing principal
           dimensions.

Fig. 5
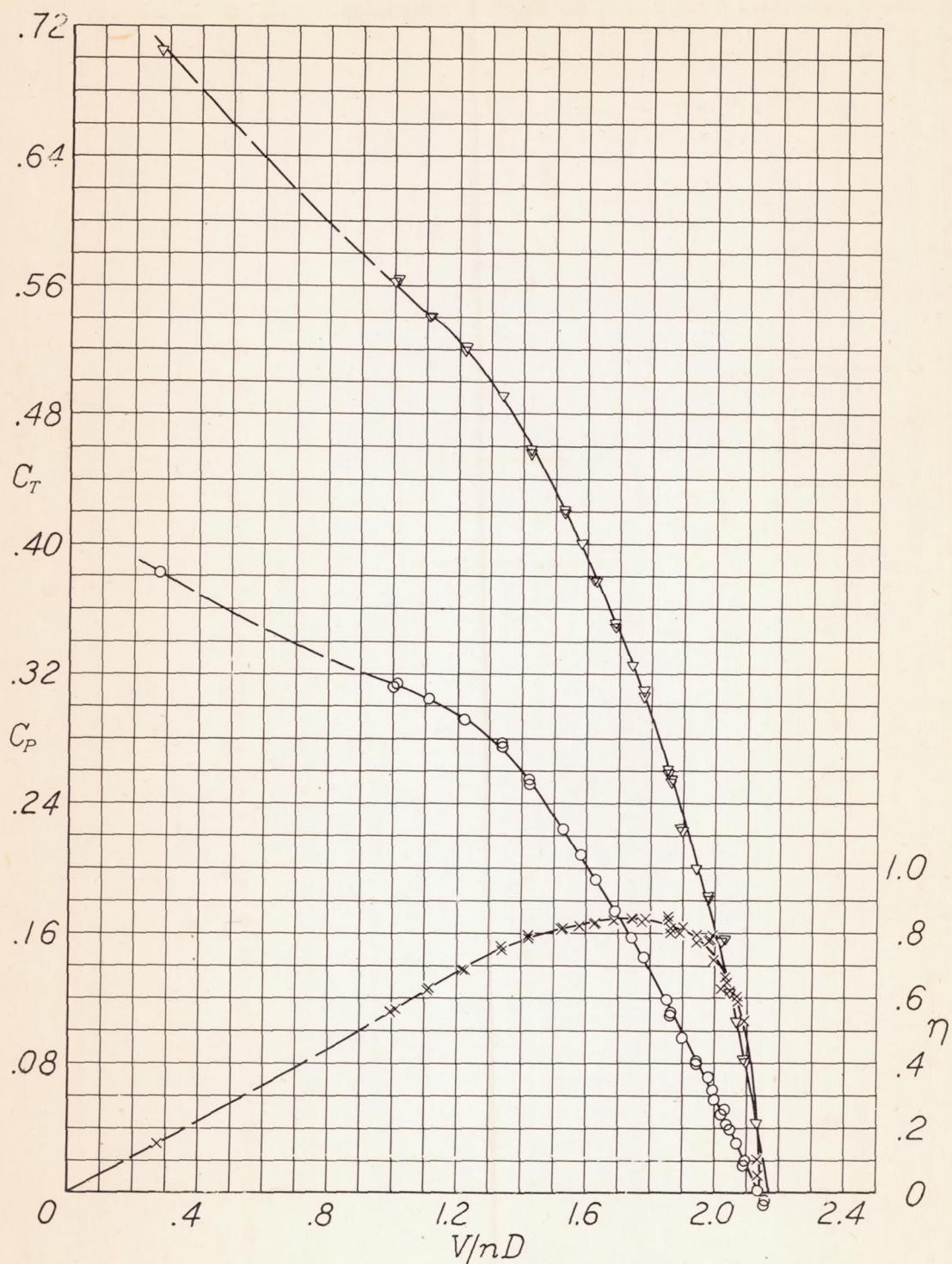
Figure 6.- Typical test results (propeller 512, $\beta_F = 40.0°$ and $\beta_R = 40.4°$ at 0.75R).
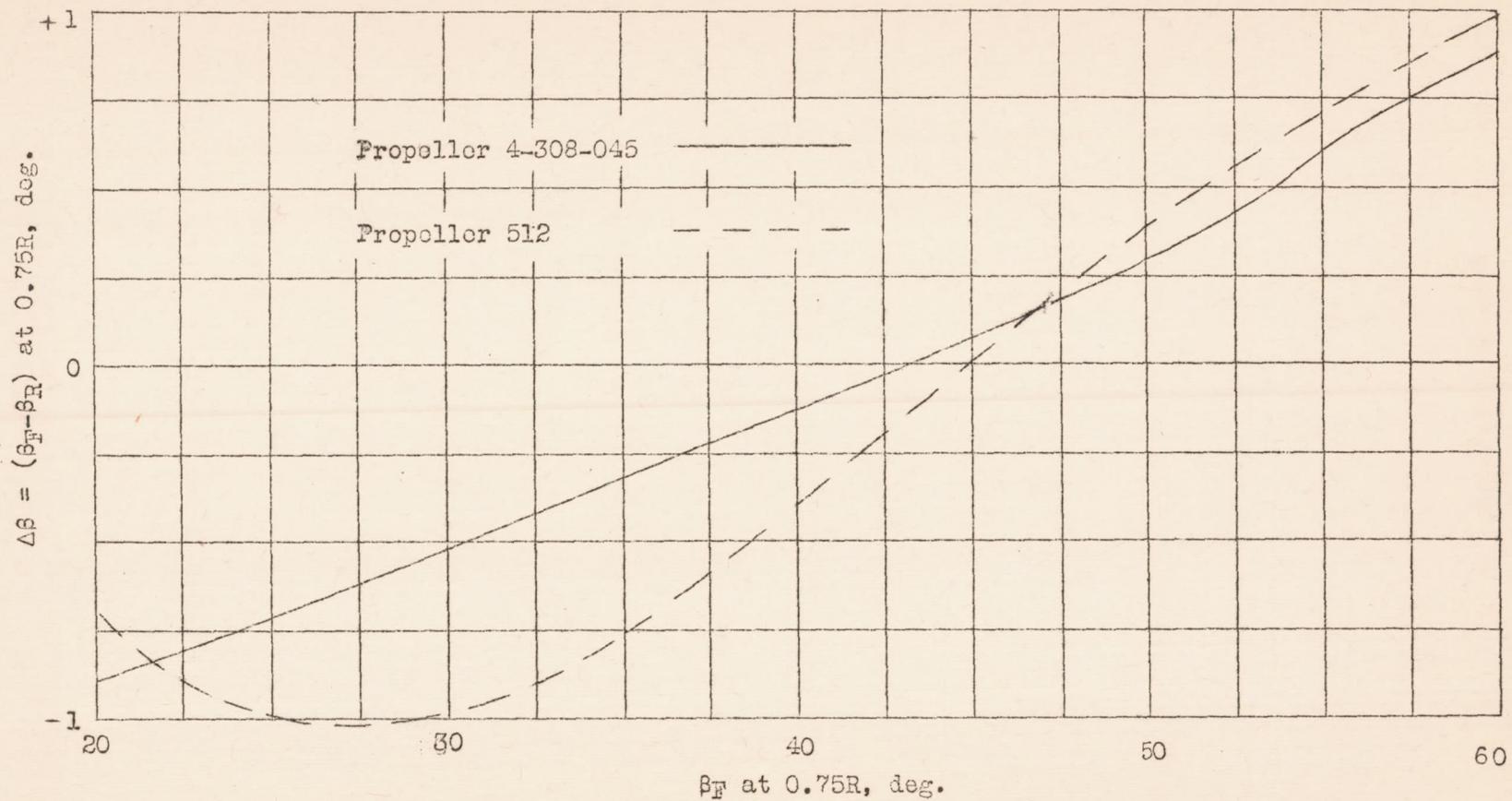
Figure 7.- Difference between front and rear blade angles to obtain equal power coefficient C_p at peak efficiency.

Fig. 7
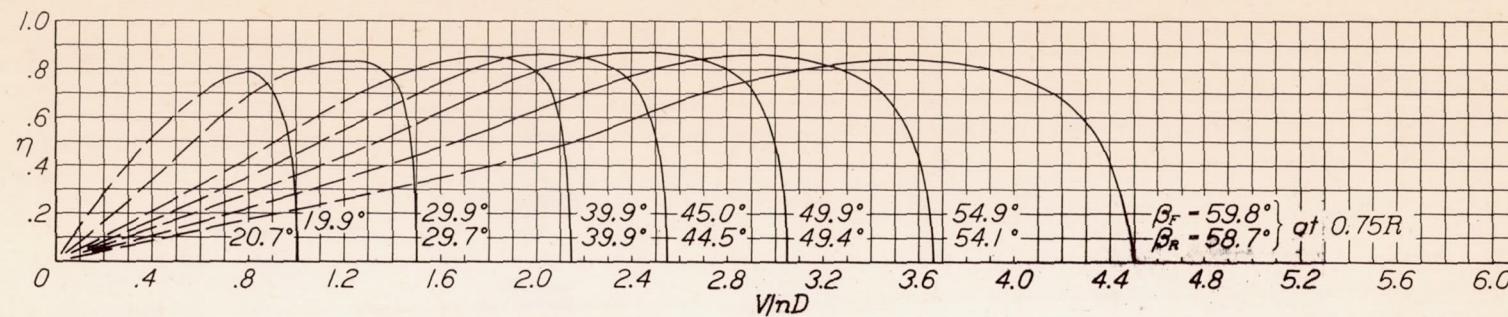
Figure 8.- Efficiency curves for six-blade counterrotating pusher propeller 4-308-045.
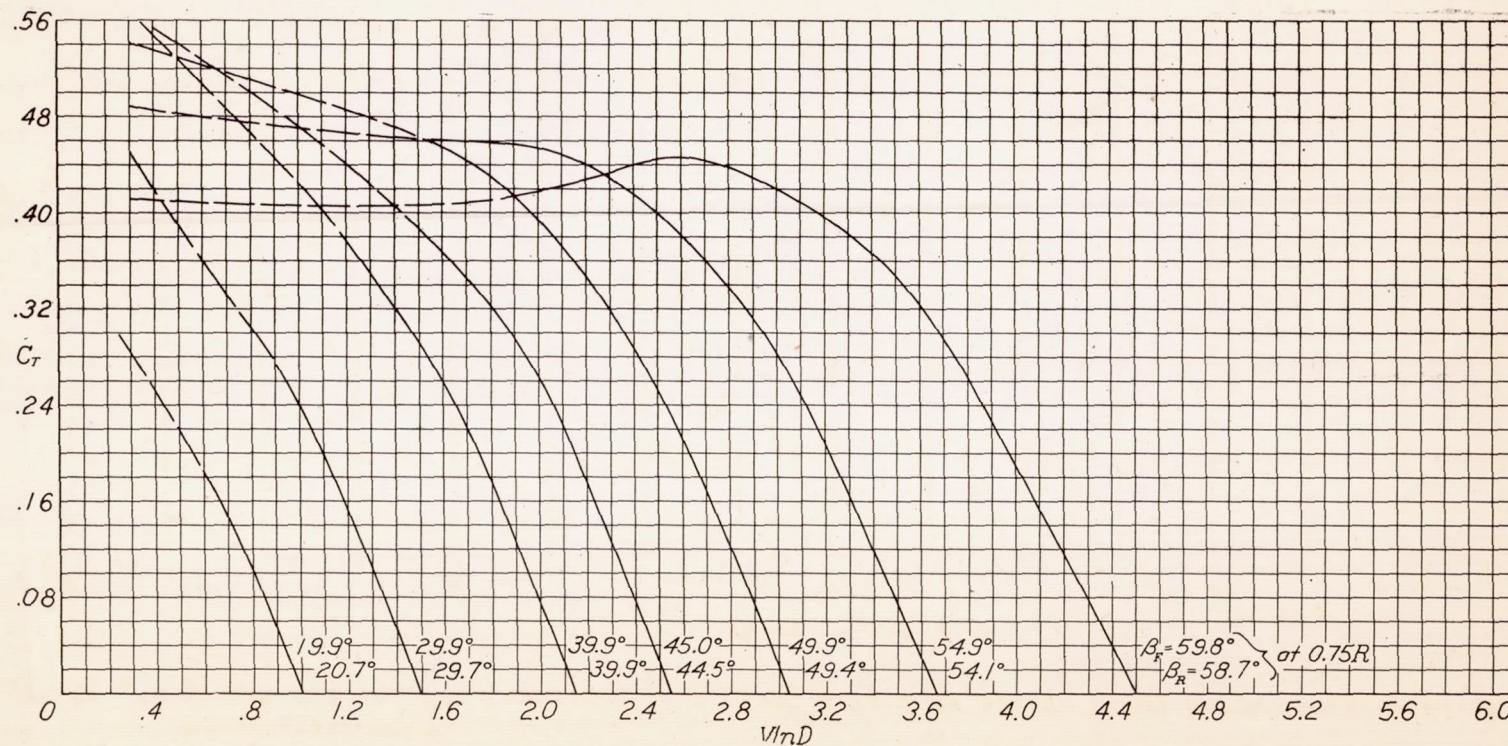
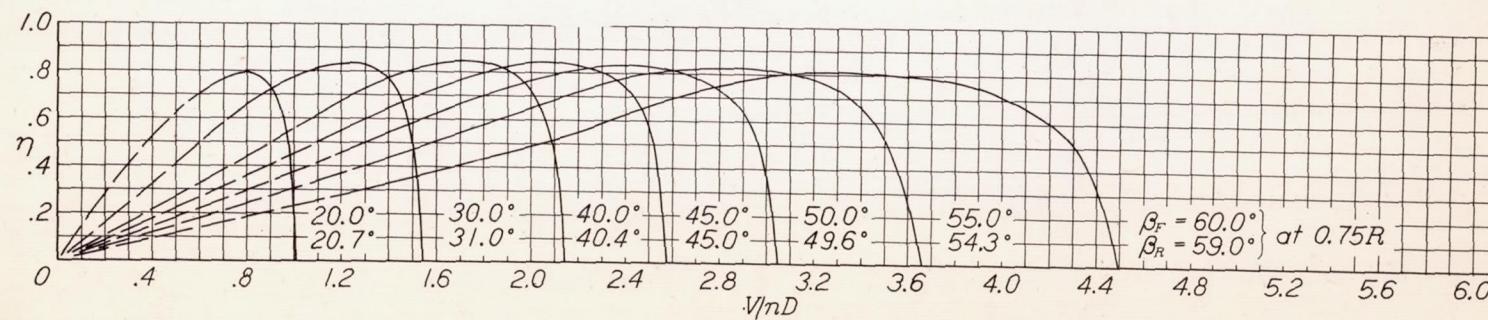Figure 9.- Thrust-coefficient curves for six-blade counterrotating pusher propeller 4-308-045.
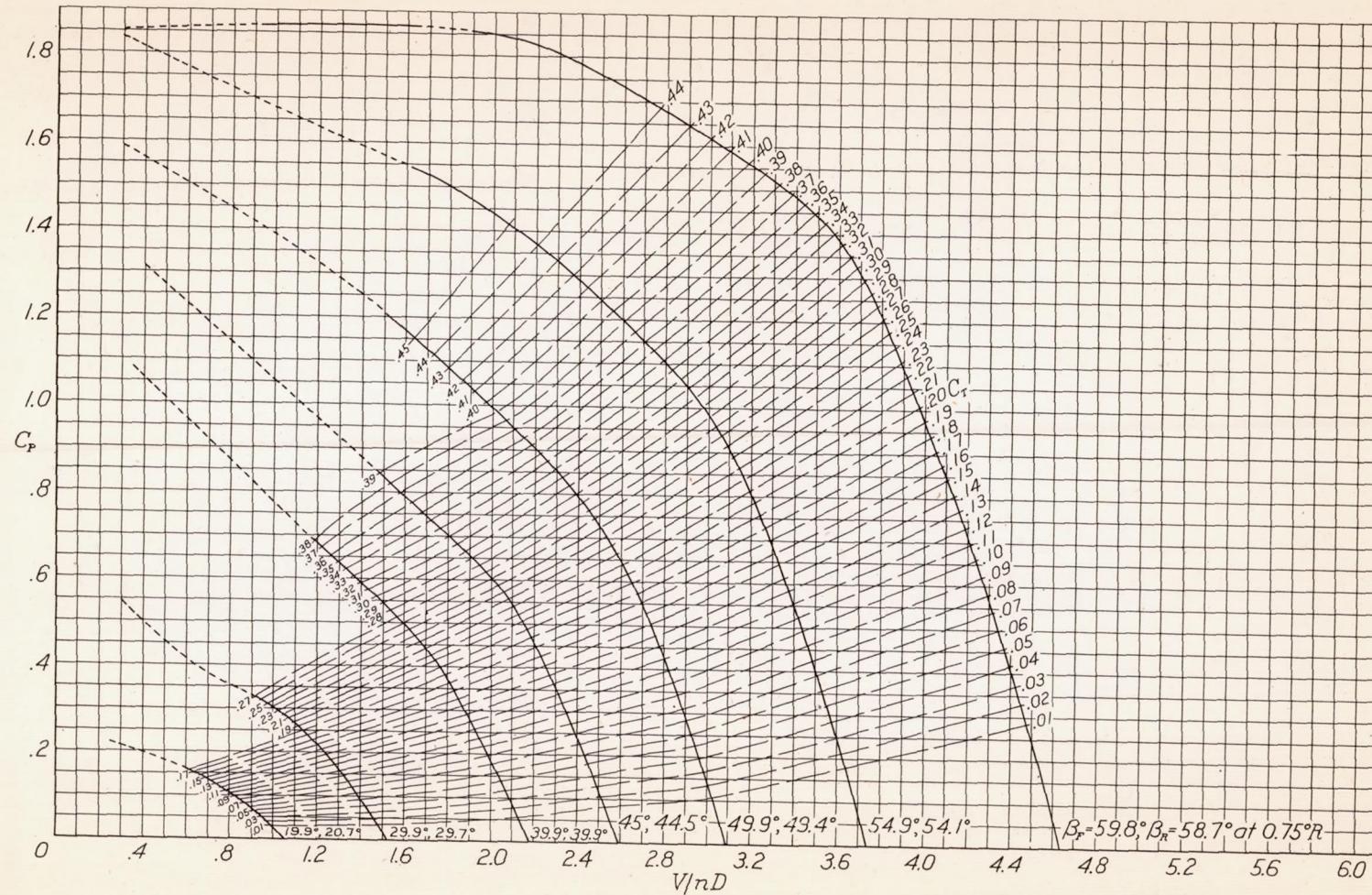
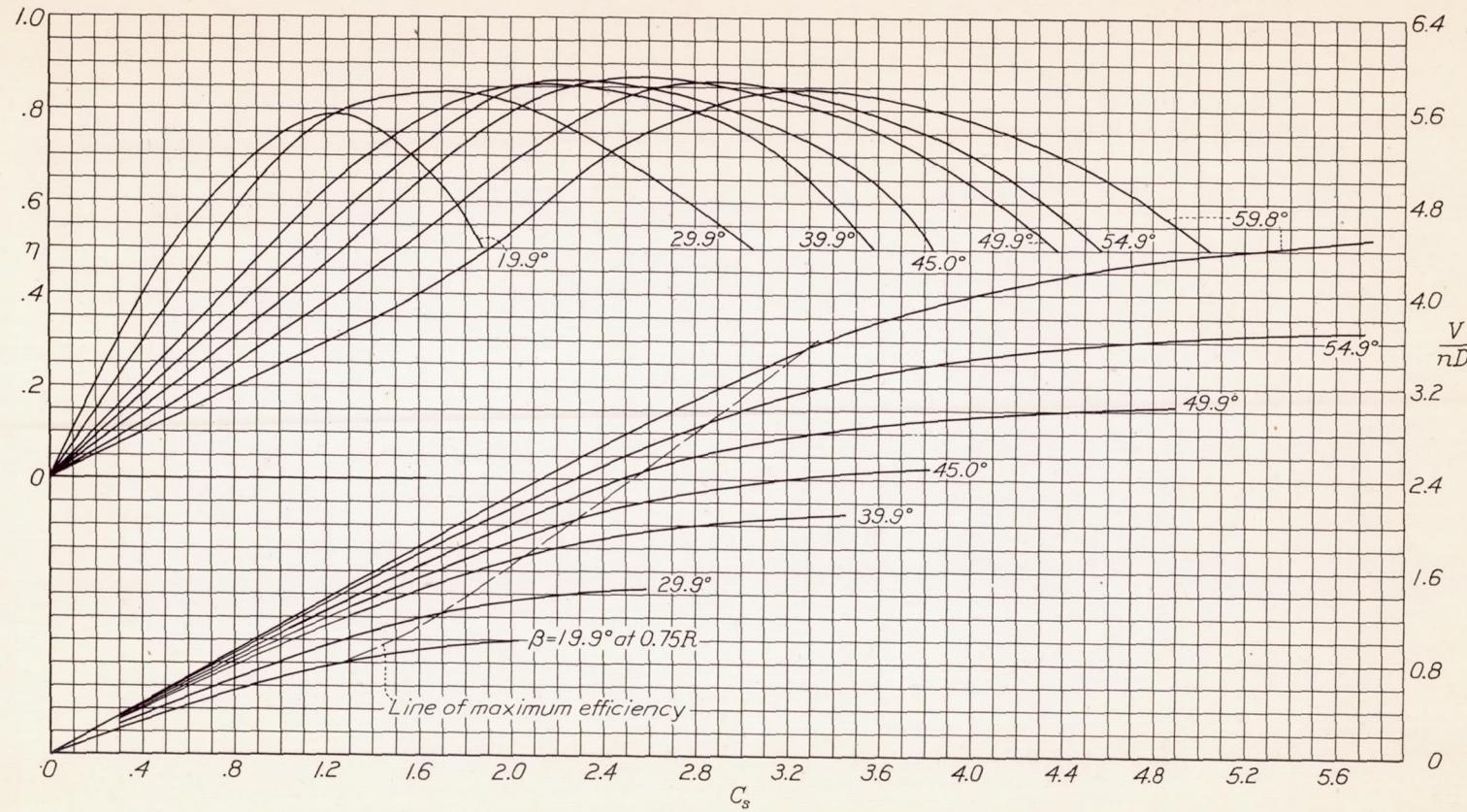Figure 10.- Power-coefficient curves for six-blade counterrotating pusher propeller 4-308-045.

Fig. 10

NACA
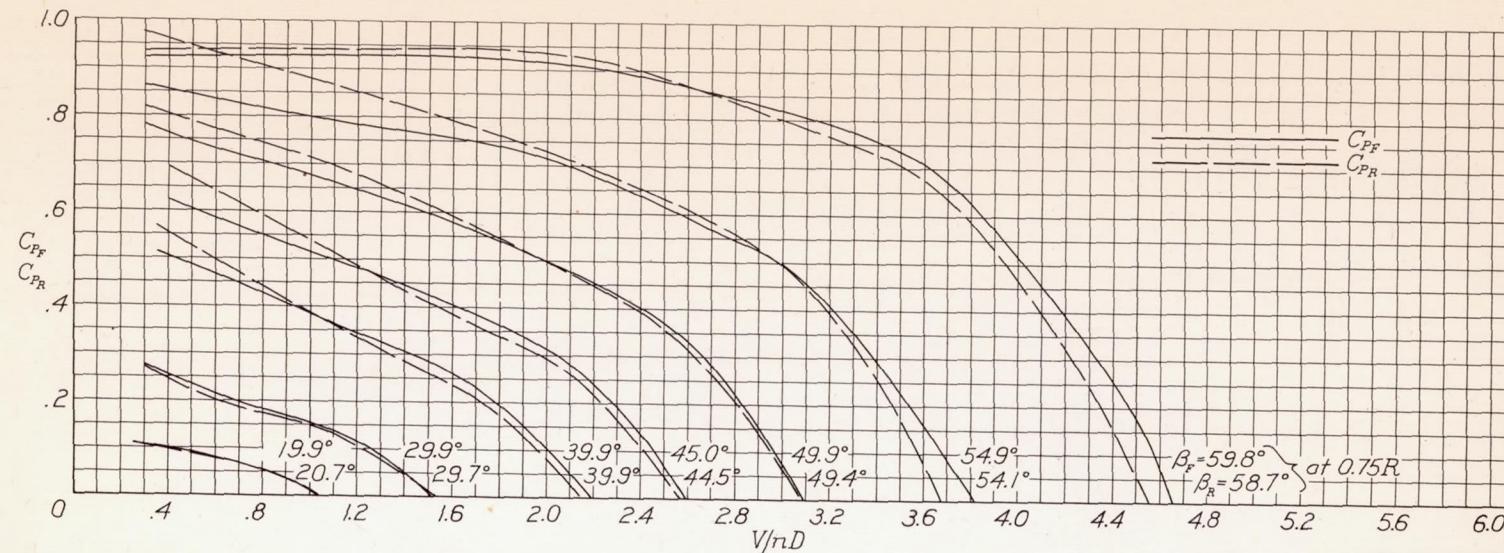
Figure 11.- Individual power-coefficient curves for six-blade counterrotating pusher propeller 4-308-045.

Figure 13.- Efficiency curves for six-blade counterrotating pusher propeller 512.

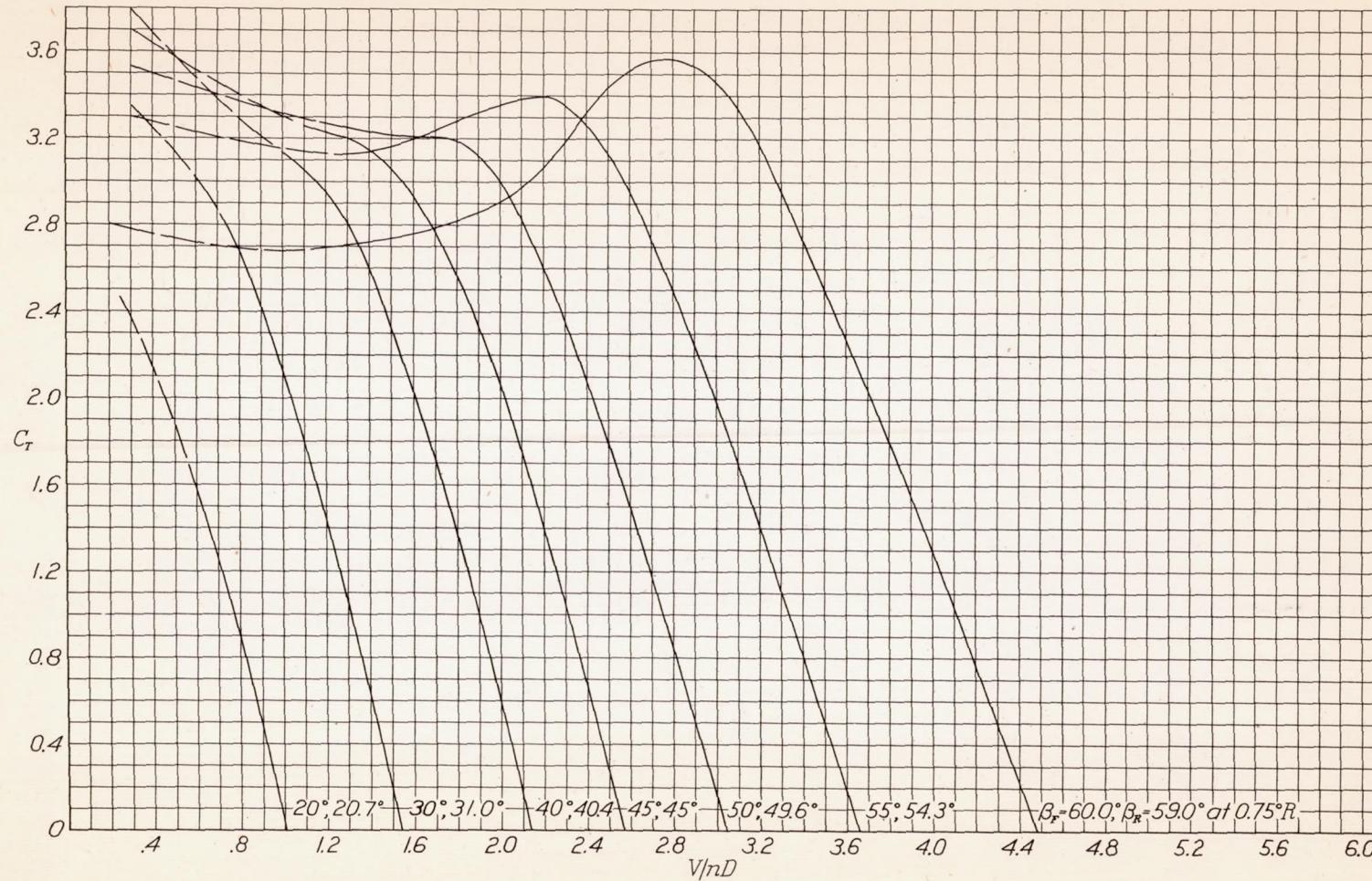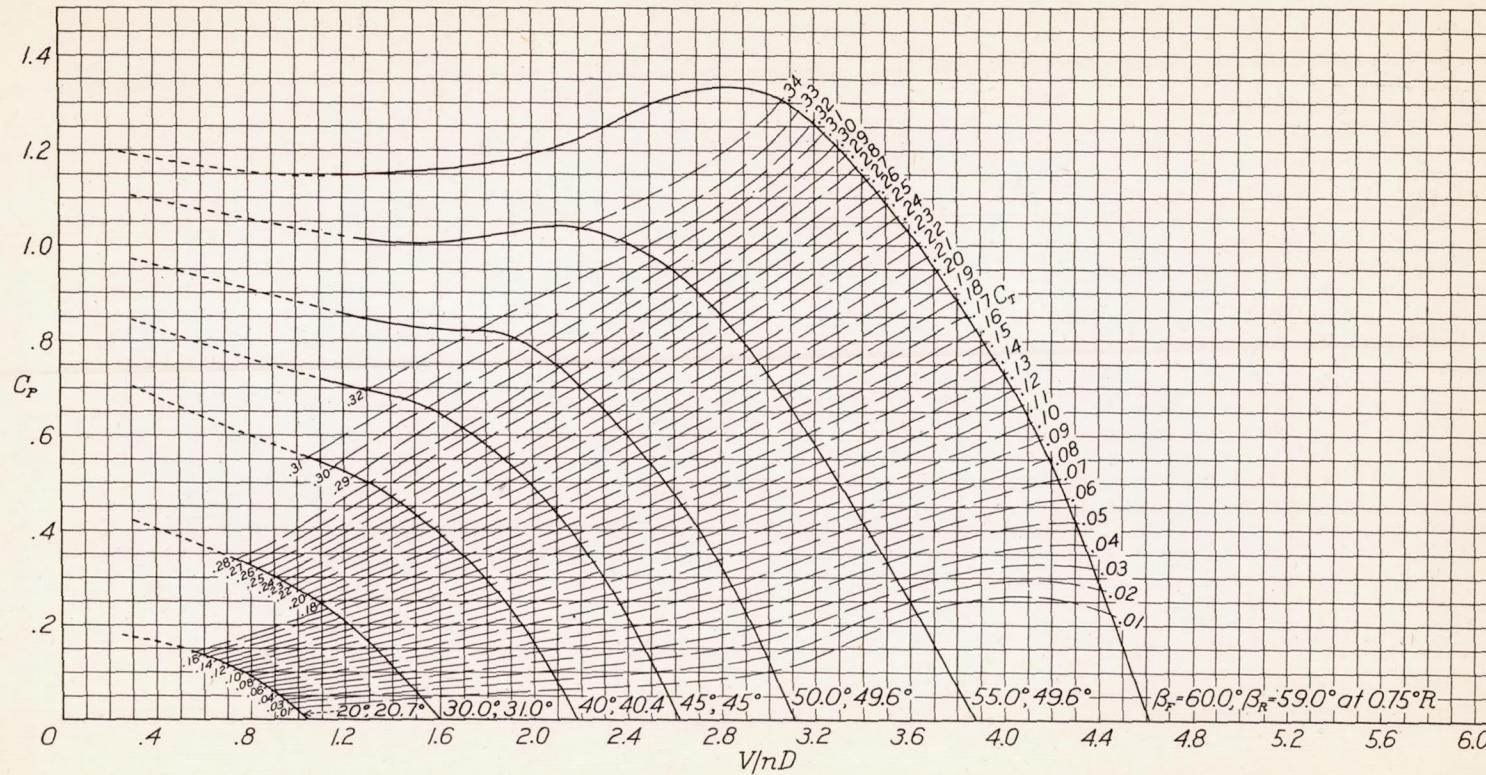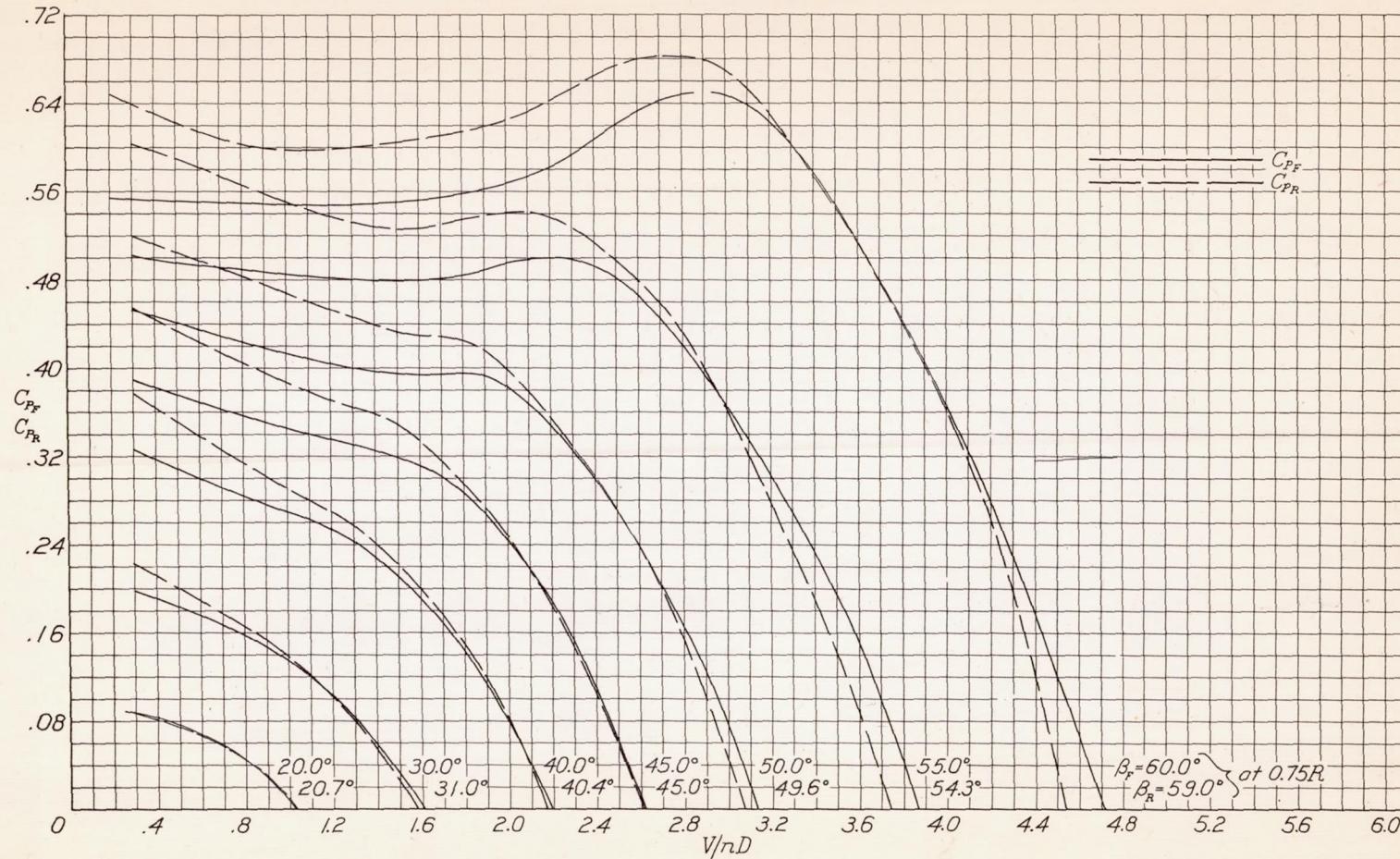Figure 12.- Design chart for six-blade counterrotating pusher propeller 4-308-045.

Fig. 12

C_T

$20°,20.7°$ $30°,31.0°$ $40°,40.4°$ $45°,45°$ $50°,49.6°$ $55°,54.3°$ $\beta_F=60.0°,\beta_R=59.0°$ at $0.75°R$

V/nD

Figure 14.- Thrust-coefficient curves for six-blade counterrotating pusher propeller 512.

Fig. 14

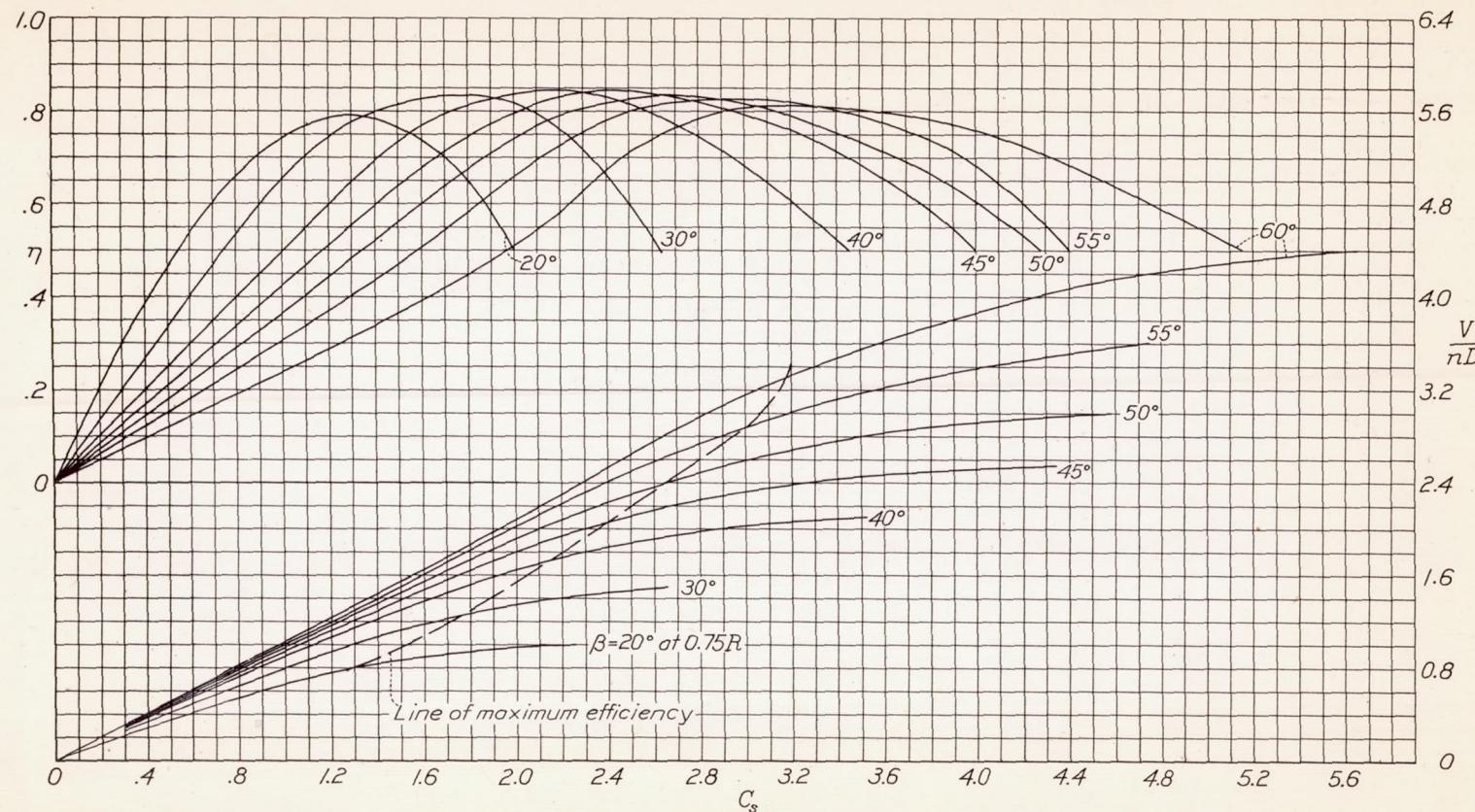Figure 15.- Power-coefficient curves for six-blade counterrotating pusher propeller 512.

Fig. 15

Figure 16.- Individual power-coefficient curves for six-blade counterrotating pusher propeller 512.

Fig. 16

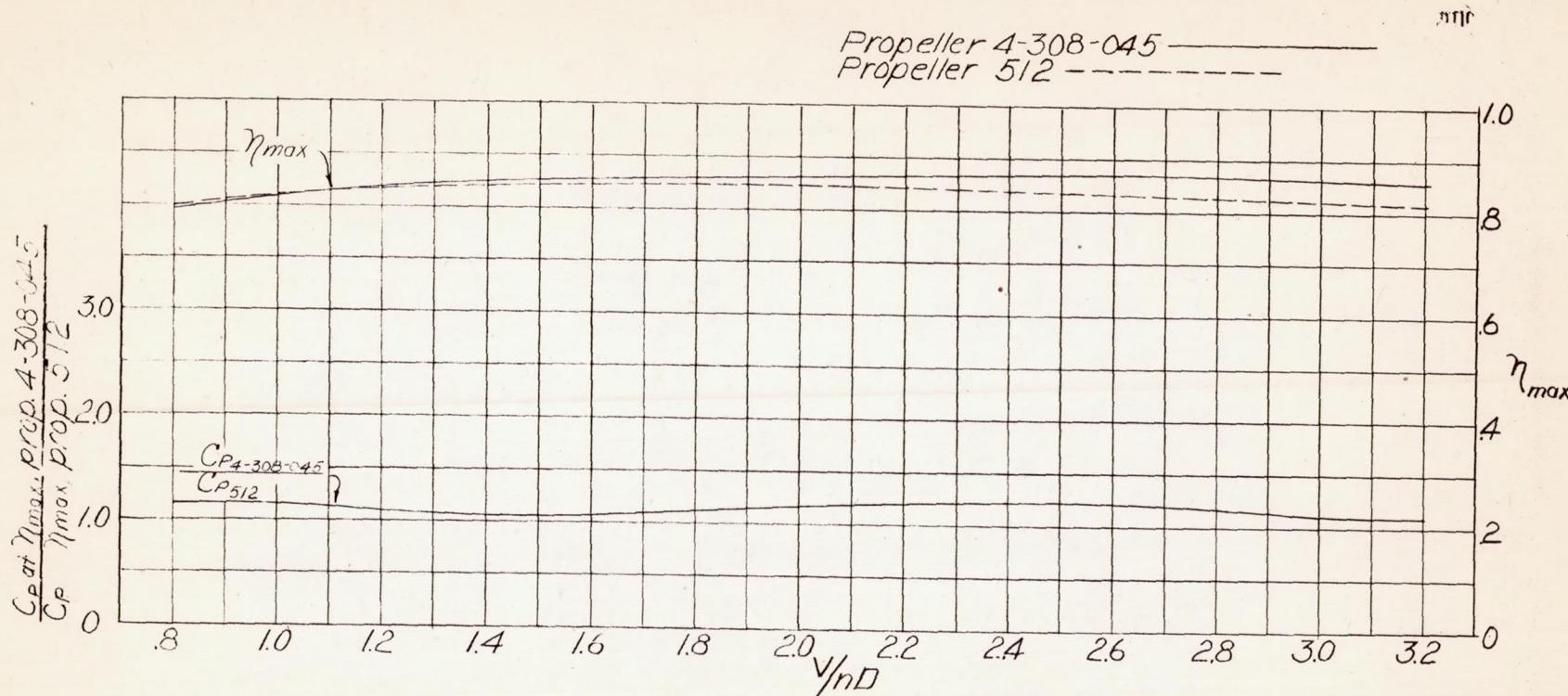Figure 17.- Design chart for six-blade counterrotating pusher propeller 512.

Fig. 17

Figure 18.— Variation of envelope efficiencies and power-coefficient ratios at peak efficiencies for counterrotating pusher propellers 4-308-045 and 512.
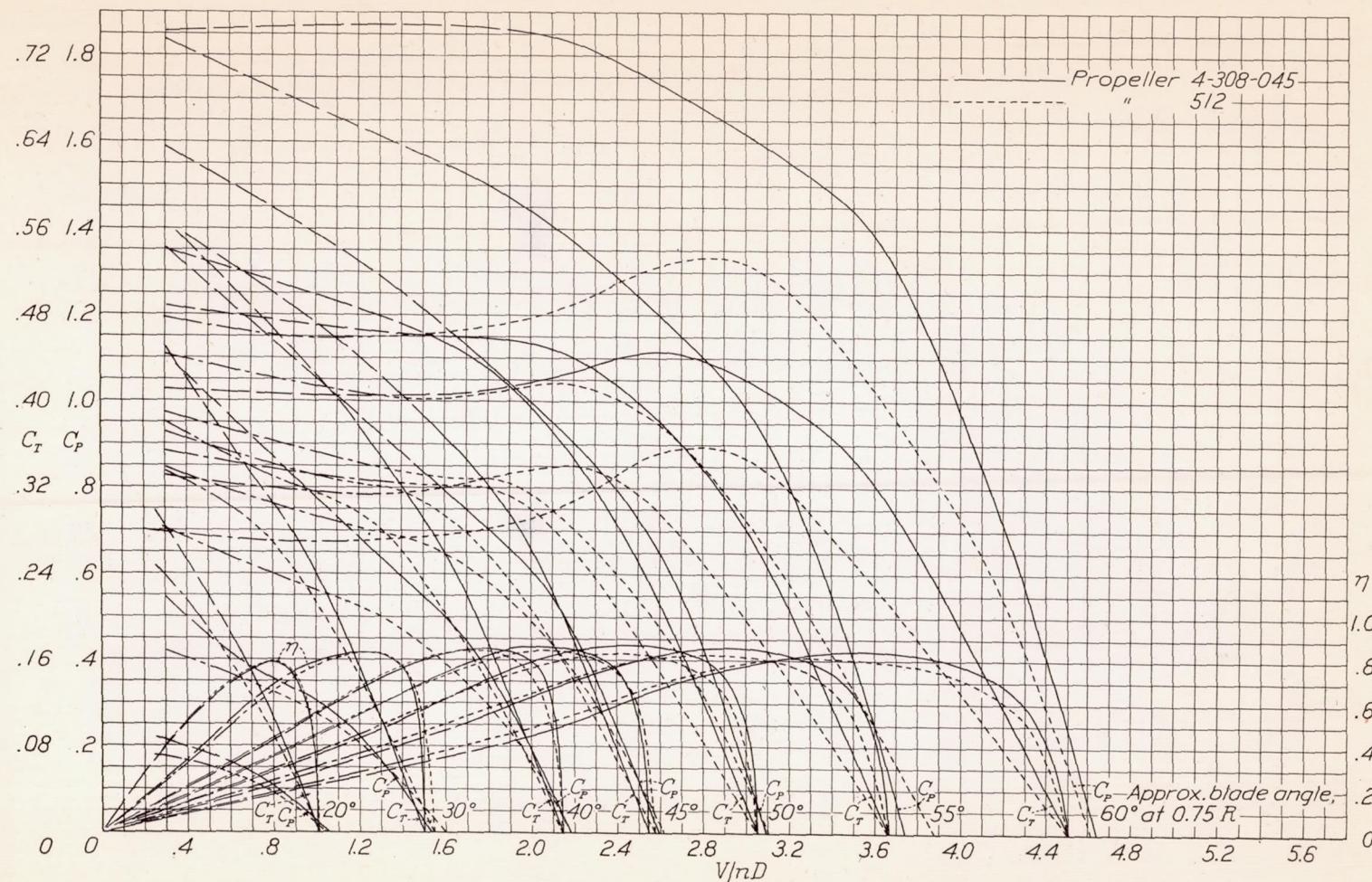
Fig. 18

Figure 19.- Composite of characteristic curves for six-blade counterrotating pusher propellers 4-308-045 and 512.

Fig. 19